Growth, structural and electrical properties of polar ZnO thin films on MgO (100) substrates

Magdalena G. Nistor, Nicolae Bogdan Mandache, Jacques Perriére, Christian Hébert, Florin V. Gherendi, Wilfried Seiler

Growth, structural and electrical properties of polar ZnO thin films on MgO (100) substrates

M. Nistor [a,*], N.B. Mandache [a], J. Perrière [b], C. Hebert [b], F. Gherendi [a], W. Seiler [c]

[a] National Institute for Lasers, Plasma and Radiation Physics, Plasma Physics and Nuclear Fusion Laboratory, L22 P.O. Box. MG-36, 77125 Bucharest-Magurele, Romania
[b] Institut des Nanosciences de Paris, Université Pierre et Marie Curie-Paris 6, CNRS UMR 7588, Campus Boucicaut, 140 rue de Lourmel, 75015 Paris, France
[c] Laboratoire d'Ingenierie des Materiaux, Ecole Nationale Supérieure des Arts et Métiers, CNRS UMR 8006, 151 Boulevard de l'Hopital, 75013 Paris, France

A B S T R A C T

ZnO films have been grown on (100) oriented MgO substrates by pulsed-electron beam deposition in the room temperature to 500 °C range. Highly (00·2) textured films are obtained for a growth temperature higher than 200 °C, and epitaxial films are formed at 500 °C with the following epitaxial relationships: $(1\text{-}1\cdot0)_{ZnO}$ // $(110)_{MgO}$ and $(11\cdot0)_{ZnO}$ // $(110)_{MgO}$, despite the difference in symmetry between film and substrate. The low temperature resistivity curves evidenced a metal–semiconductor transition for the ZnO films grown in the 300 to 500 °C range which has been interpreted in the frame of the model of conductivity in disordered oxides.

Keywords:
Epitaxial zinc oxide thin films
Metal-semiconductor transition
Pulsed-electron beam deposition
Channel-spark

1. Introduction

While the growth of c-axis epitaxial ZnO films on crystalline substrates like sapphire presenting the rhomboedral symmetry has been and is nowadays the subject of numerous works [1], the formation of ZnO films on single crystal substrates presenting a different structural symmetry is not so well documented. The formation of non polar ZnO films, i.e. ZnO films with their c-axis in the plane parallel to the substrate, would however lead to interesting applications [2,3]. Motivated by this aspect, the growth of ZnO films on cubic substrates has been studied, in particular on $SrTiO_3$ single crystal substrates according to the fact that a high density, two dimensional electron gas with unique electrical and thermal properties forms at the interface between $SrTiO_3$ and other oxides [3,4]. The growth of non polar m oriented (11·0) ZnO films on (001) $SrTiO_3$ substrates has been thus reported [3,4], while the classical polar (00·2) ZnO growth is observed on (111) oriented $SrTiO_3$ [5].

In the case of ZnO films on MgO single crystal substrates, the situation appears rather confusing, with results which in terms of film orientation not only depend upon the substrate orientation, but also on the growth method, and experimental conditions. Indeed, films with multiple textures, or m-axis or c-axis oriented ZnO films can be obtained depending upon growth parameters [2,6–8]. This underlines the difficulties to obtain high crystalline quality ZnO thin films with a single epitaxial relationship with the MgO single crystal substrate. The epitaxial growth is not trivial, due to differences in crystallographic symmetries of the hexagonal ZnO network ($a = 0.3249$ nm and $c = 0.5206$ nm) and the cubic MgO ($a = 0.421$ nm).

We have studied the formation, structure and electrical properties of ZnO films grown on (100) oriented single crystal MgO substrates, by the pulsed-electron beam deposition method (PED). This thin film growth technique [9–13], conceptually similar to the pulsed laser deposition, differs by the use of an intense pulsed electron beam to ablate the target material instead of a laser beam. Oxide films are easily grown by PED, with a good control of the surface morphology, cationic composition, oxygen stoichiometry and crystalline structure of the films [9–14]. Our main objective was to determine the pertinent parameters governing the ZnO film orientation and epitaxial relationships with MgO substrates, and to correlate their structural characteristics with their electrical properties. We evidenced the (00·2) ZnO growth on (100) MgO substrates, as well as the heteroepitaxial growth of ZnO films. Depending on the growth temperature, variations in the electrical properties were observed for the ZnO films grown on (100) MgO substrates. The resistivity curve shows a semiconducting behaviour for the films grown at room temperature, while the films grown in the 300 to 500 °C range show a metallic conductivity at room temperature followed at lower temperatures by a metal–semiconductor transition (MST), as was already observed in epitaxially ZnO films on Al_2O_3 single crystal substrates grown by PED [14]. This behaviour was interpreted in the frame of the quantum corrections to conductivity in a disordered medium [15].

* Corresponding author. Tel./fax: +40 214574490.
E-mail address: mnistor@infim.ro (M. Nistor).

2. Experimental details

The ZnO films were grown on (100) oriented MgO substrates by the PED method [9,16,17]. The PED set-up consists of a pulsed electron beam source in the channel-spark discharge configuration and a vacuum chamber for the thin film growth. The channel-spark discharge configuration consists of a hollow cathode, a dielectric capillary tube (6 mm diameter and 100 mm length) and the vacuum chamber as the grounded anode.

A pulsed intense electron beam is produced when an external capacitor of 16 nF, charged at 15 kV, is discharged between the hollow cathode and the anode. The pulsed electron beam has 100 ns full width at half maximum (FWHM), a fluence of 2.5 J/cm^2 and a repetition rate of 1 Hz. The electron beam interacts at an angle of 45° with the ZnO target, in Ar gas at a pressure of 1 Pa and a residual oxygen pressure equal to 10^{-3} Pa. The MgO (100) substrates were placed parallel to the target at a distance of 40 mm. ZnO thin films were grown under a controlled substrate temperature in the room temperature to 500 °C range. After deposition the films were cooled down under the argon pressure used for the growth.

The thickness and composition of the films were measured by Rutherford backscattering spectrometry (RBS) using the 2 MeV Van de Graaff accelerator at the Institut des Nanosciences de Paris (Université Paris 6). The structural characterizations of the ZnO films were carried out by X-ray diffraction (XRD) analyses using a four-circle diffractometer (Philips Xpert MRD) with the Cu Kα radiation (λ = 0.154 nm) at the Laboratoire d'Ingenierie des Materiaux (Ecole Nationale Supérieure des Arts et Métiers). Analyses in the symmetric Bragg–Brentano geometry were used to determine the axis parameters and possible textures of the films. The in-plane epitaxial relationships between the ZnO films and MgO substrates were studied by asymmetric X-ray diffraction from the measurements of pole figures for selected XRD peaks of the films and substrate. The resistivity of ZnO films as a function of temperature (from room T down to liquid He) was obtained by the standard dc four-probe measurements.

3. Results

The parameters of the PED method were optimized in order to obtain dense and smooth ZnO films free from any particulates at their surface, as it has been previously established [9], with the film thickness in the 50–100 nm range. Fig. 1 represents a typical RBS spectrum which shows the formation of a stoichiometric and uniform ZnO film. However, due to the accuracy of the RBS analysis for the determination of the content in light elements (like oxygen), i.e. about 5%, we cannot exclude a slight oxygen deficiency in the ZnO films. Such a possible deviation in stoichiometry could be due to the fact that these films are grown under a quite low oxygen pressure that usually involves an unbalanced incorporation of cations and oxygen atoms into the film [18,19]. This RBS spectrum does not show the presence of elements other than Zn, O and Mg, i.e. the incorporation during the PED growth of foreign atoms which could play an important role in the transport properties of the films [20,21] is not evidenced by RBS.

X-ray diffraction patterns were recorded for the ZnO films grown on (100) MgO substrates at room T, 300 and 500 °C. Films grown at T<200 °C were found amorphous. Fig. 2 shows typical XRD patterns for films grown at 300 and 500 °C and for the MgO substrate, respectively. The scan shows the presence of the (00·2) reflection peak and its harmonics characteristic of the ZnO wurtzite structure, along with the (100) MgO substrate reflections, indicating that the ZnO film is highly c-axis oriented, a very small (10·0) ZnO peak being observed only at 2θ = 31.7°. Note that the (111), (200), (220) and (311) Au peaks observed in the XRD pattern of the ZnO film are due to the Au contacts deposited on the film for resistivity measurements.

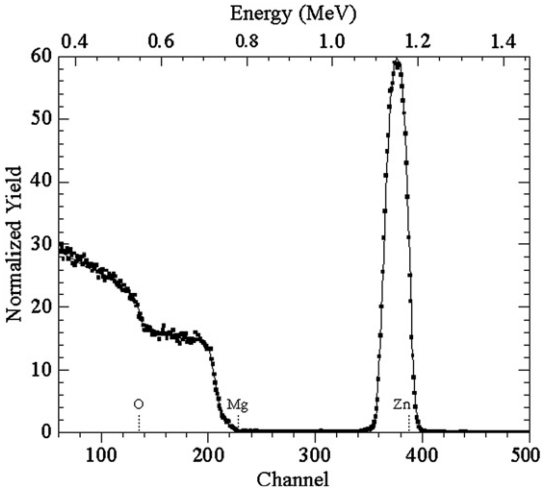

Fig. 1. A typical RBS spectrum recorded for a ZnO film grown by PED on the (100) MgO substrate at 300 °C.

Moreover, the absence of any additional peaks in the XRD patterns rules out the presence of spurious crystalline phases in the ZnO films.

The c-axis parameters obtained from the XRD patterns, the values of crystallite size d (coherence length) deduced from the (00·2) ZnO line width (the Scherrer formulae) and the FWHM values of the rocking curves of the (00·2) reflection peaks are presented in Table 1 for the ZnO films grown on MgO substrates at 300 and 500 °C substrate temperatures. The FWHM of the (00·2) ZnO rocking curves show a decrease from 4.8° at 300 °C to 2.4° at 500 °C. Moreover, the ZnO c axis values are larger than the bulk value (0.5206 nm), the difference decreasing with increasing growth temperature, which could be explained by a decreasing defect density in the films as the growth temperature increases. All these results prove an enhancement of the crystalline quality of the ZnO films with T, i.e. a decrease of the defect density in films with increasing growth T, as it is generally observed in the case of ZnO film growth [1,14,22].

XRD pole figures were observed only for films grown at T>300 °C. Fig. 3 represents a typical pole figure of the (10·3) ZnO plane, recorded for 2θ = 62.8°, for a ZnO thin film grown on the (100) MgO substrate at 500 °C. Twelve well-defined poles are observed at a declination angle ψ equal to 31.6°, i.e. the value expected for the (10·3) plane of the ZnO wurtzite structure in the case of a (00·2) texture. In addition, the poles located at ψ = 45° with a four fold

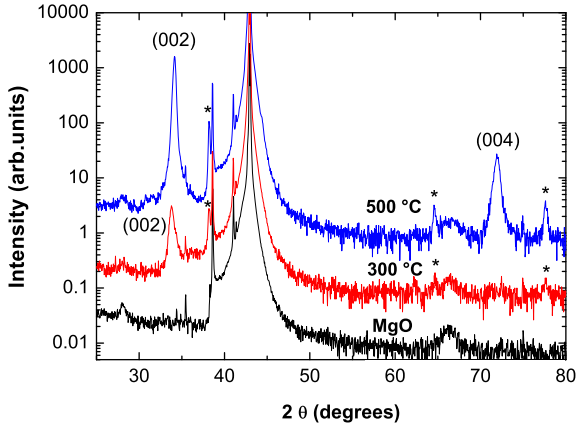

Fig. 2. X-ray diffraction patterns for the ZnO thin films grown on the (100) MgO substrate at 300 and 500 °C and the (100) MgO substrate, respectively. The (111), (200), (220) and (311) Au peaks are marked by *.

Table 1
Structural parameters of the ZnO films grown at 300 and 500 °C on (100) MgO substrates.

Substrate temperature	C-axis parameter (nm)	Crystallite size (nm)	FWHM rocking curve (°)
300 °C	0.5307	14	4.8
500 °C	0.5253	28	2.4

symmetry (Fig. 3) correspond to the (220) plane of the MgO substrate, and are observed owing to the diffraction angle $2\theta = 62.8°$ of this plane.

The azimuthal positions of the (10·3) ZnO poles in respect with the MgO substrate (110) poles lead to the following in-plane relationships:

$$(1{-}1{\cdot}0)_{ZnO} \,//\, (110)_{MgO} \quad \text{and} \quad (11{\cdot}0)_{ZnO} \,//\, (110)_{MgO}.$$

Owing to the six-fold in plane symmetry of the ZnO, these two relationships lead to the 12 poles which are observed in Fig. 3. To highlight these epitaxial relationships, Fig. 4a and b represents the in-plane atomic arrangement corresponding to the interface (00·2) ZnO film on the (100) MgO substrate. In this schema, we have taken into account the rumpling phenomenon on the MgO surface. Indeed the MgO substrate heated under reduced oxygen pressure can undergo a rumpling phenomenon, i.e. atomic displacements of the O versus Mg atoms of the free surface plane, leading thus to the formation of an oxygen atomic plane at the surface [23]. The last MgO plane can thus be considered as an electronegative plane, and it has been schematized in Fig. 4 by the oxygen atoms of the (100) MgO plane. Accordingly, the first deposited ZnO plane is an electropositive plane, i.e. a (00·2) Zn plane has been thus considered in these figures.

The epitaxial relationships presented in Fig. 4 can be explained in the frame of the domain matching epitaxy or extended atomic distance mismatch approach [24], in which the m lattice units of the film match with p lattice units of the substrate. The values of m and p are defined as the minimum integers which satisfy the relation:

$$m\, d_{ZnO} = p\, d_{MgO} \quad \text{or} \quad d_{ZnO} / d_{MgO} \approx p / m$$

with d_{ZnO} and d_{MgO} being the respective atomic distances in the ZnO and MgO parallel directions. The corresponding lattice mismatch δ can then be defined by:

$$\delta = 2\left[m\, d_{ZnO} - p\, d_{MgO}\right] / \left[m\, d_{ZnO} + p\, d_{MgO}\right].$$

Considering the two aligned directions in Fig. 4, and the values of d_{ZnO} along the (1-1·0) and (11·0) directions (0.2814 and 0.3249 nm respectively), to compare with d_{MgO} (0.5954 nm), the resulting matching and lattice mismatches are given in Table 2. The limited values of the lattice mismatch along the two directions in Fig. 4 can justify the epitaxial relationships observed in this work.

In order to check how the growth of ZnO films on (100) MgO single crystal substrates influence the electrical properties of the films, temperature variable resistivity measurements were performed. Fig. 5 shows the normalized resistance (R(T)/R(300 K)) measured in the temperature range 4–300 K for films grown at room T, 300 and 500 °C, respectively. The absolute values of resistivities measured at 300 K are: 0.0122 Ωcm for the ZnO/MgO film grown at RT; 0.0033 Ωcm for the ZnO/MgO film grown at 300 °C and 0.0023 Ωcm for the ZnO/MgO film grown at 500 °C.

The film grown at room T shows only a negative coefficient of R(T) which is characteristic of semiconducting behaviour. On the contrary, minima are observed on the curves corresponding to the 300 and 500 °C growth temperatures. In fact, from room T to the normalized resistance minimum, the temperature coefficient of resistivity is

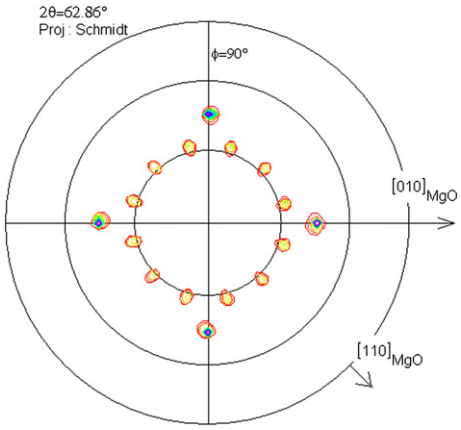

Fig. 3. Pole figure of the (10·3) ZnO plane for the ZnO film grown on the (100) MgO substrate at 500 °C.

positive (metallic behaviour), while for the lowest T it is negative (semiconducting behaviour). Such a metal–semiconductor transition has been reported for ZnO films doped with various elements, grown by different deposition methods [20,21,25–30], but pure undoped ZnO films grown with the same methods and same experimental conditions did not present such a metal–semiconductor transition (MST). Recently, a metallic behaviour and a MST have been reported in undoped ZnO films grown on c-cut sapphire substrates by PED [14], spray pyrolysis [30], the transition temperature being at about 170 K and around 420 K, respectively.

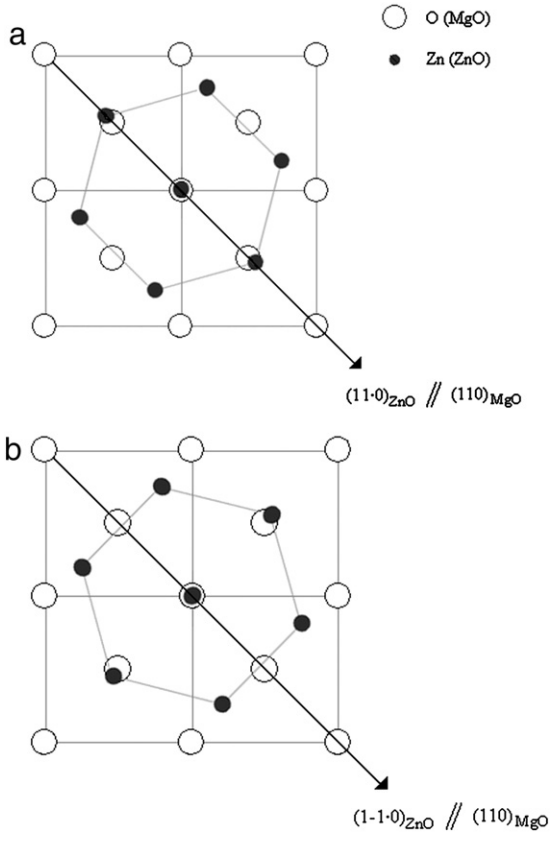

Fig. 4. Schematic representation of the interface between the (00.2) ZnO film and the (100) MgO substrate with the corresponding in-plane relationships: (a) $[1\text{-}1{\cdot}0]_{ZnO}$ // $[110]_{MgO}$ and (b) $[11{\cdot}0]_{ZnO}$ // $[110]_{MgO}$.

Table 2
The domain matching epitaxy relationships and the lattice mismatch for the corresponding in-plane orientations of the ZnO films on the (100) MgO substrate.

In-plane orientation	Domain matching epitaxy relationships	Lattice mismatch
$(1\text{-}1\cdot0)_{ZnO}$ // $(110)_{MgO}$	$2\ d_{ZnO} \approx 1\ d_{MgO}$	$\delta = 5.60\%$
$(11\cdot0)_{ZnO}$ // $(110)_{MgO}$	$9\ d_{ZnO} \approx 5\ d_{MgO}$	$\delta = 1.76\%$

Fig. 6 a shows the Arrhenius plot of the resistivity of the ZnO film grown on a MgO substrate at room T. As it is shown in the inset, in the temperature range 294 to 185 K ($\Delta T = 109$ K) the resistivity follows an Arrhenius law versus temperature written in the form: $\ln\rho = \ln\rho_0 + (E_a/k_B)\ T^{-1}$, and the estimated activation energy is $E_a = 2.65$ meV. For $T < 185$ K the resistivity increases and a pronounced curvature is observed in the Arrhenius plot, as it is generally observed in semiconducting oxides [19]. A classical explanation of this behaviour is based on a variable range hopping (VRH) mechanism related to the localization of carriers, in which $\ln \rho\ (T)$ follows a linear dependence on $T^{-1/4}$ (three dimensional VRH) [19]. However, this does not seem to be the case for the ZnO film grown at room T. Actually, as it is shown in Fig. 6b, $\ln\ \rho\ (T)$ does not present a linear variation with $T^{-1/4}$ on a significant temperature range thus a VRH mechanism does not seem to be the dominant mechanism in this low temperature domain.

The MST observed in the curve corresponding to ZnO films grown at 300 and 500 °C (Fig. 5) could be due to a variation with the temperature of the carrier density [28,29]. The density and mobility of carriers were determined by Hall effect measurements. However, the density and mobility of carriers were determined with a rather poor accuracy (about 10%), i.e. of the order of the resistivity variation due to the MST. So even if the carrier density was found roughly constant between 80 and 300 K and equal to 1.95×10^{20} cm^{-3} (for the ZnO film grown at 500 °C), it is not possible to *a priori* exclude that the MST is due to a change in the carrier concentration. However another explanation can be envisaged, similar to that proposed in the case of ZnO films grown on sapphire substrates [14]. As a result, the specific behaviour of the R(T) curves corresponding to the ZnO films grown at 300 and 500 °C was analyzed in the frame of the quantum corrections to conductivity in a disordered conductor [15]. Indeed, the metallic conductivity followed at a low temperature by a metal–semiconductor transition can originate from the weak localization and electron–electron interactions effects which are known to occur in a disordered conductor [16]. Such an approach has been already used to explain the crossover from semiconductor to metallic behaviour in various oxide materials like $SrRuO_2$ [31], $LaNiO_3$ [31,32] or even ZnO [14,21,27].

In this approach, the changes in conductivity have been analyzed and modelled [32] and the resistivity of oxide films can be described by the following expression:

$$\rho(T) = \frac{1}{\sigma_0 + a_1 T^{p/2} + a_2 T^{1/2}} + bT^2 \qquad (1)$$

where σ_0 is related to the residual resistivity ($\sigma_0 = 1/\rho_0$); $a_1T^{p/2}$ and $a_2T^{1/2}$ are the quantum corrections corresponding respectively to the weak localization effect ($a_1T^{p/2}$) and Coulomb interaction effect ($a_2T^{1/2}$) in the case of a 3D dimension disordered oxide film [32]; and bT^2 is the usual Boltzmann term. The value of p depends on the type of the interactions, p being 2 for electron–electron and 3 for electron–phonon interactions, respectively.

The resistivity curves for ZnO films grown on MgO substrates at 300 and 500 °C, respectively were fitted with the Eq. (1), as shown in Figs. 7 and 8 and the fit parameters are given in Table 3. Owing to the film thickness (>50 nm), the fit indicates that the 3D approach (Eq. (1)) describes correctly the ρ (T) behaviour for both films. Moreover, we have checked that the ρ (T) variation could not be described by a log (T) variation predicted for a 2D dimensional disordered system [15].

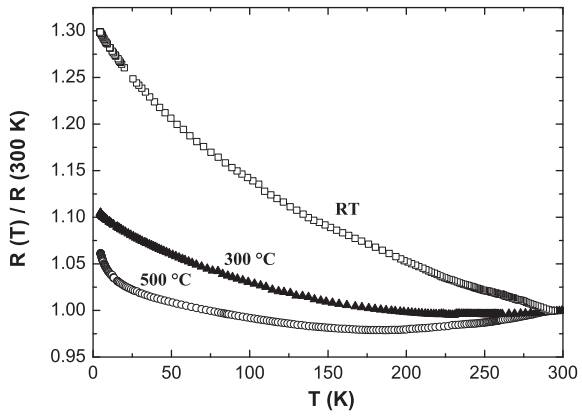

Fig. 5. Normalized resistance as a function of temperature for ZnO thin films grown on the (100) MgO substrate at room T, 300 and 500 °C.

The parameter a_1 is very small compared with a_2, and it is a clear indication that the Coulomb interaction represents the most important contribution in the quantum corrections to conductivity in disordered oxide films as it has been previously reported [27,31,32].

The model of quantum corrections to conductivity is valid when the Fermi wavelength $\lambda_F\ (2\pi / (3\pi^2 n)^{1/3})$ and the electronic mean free path

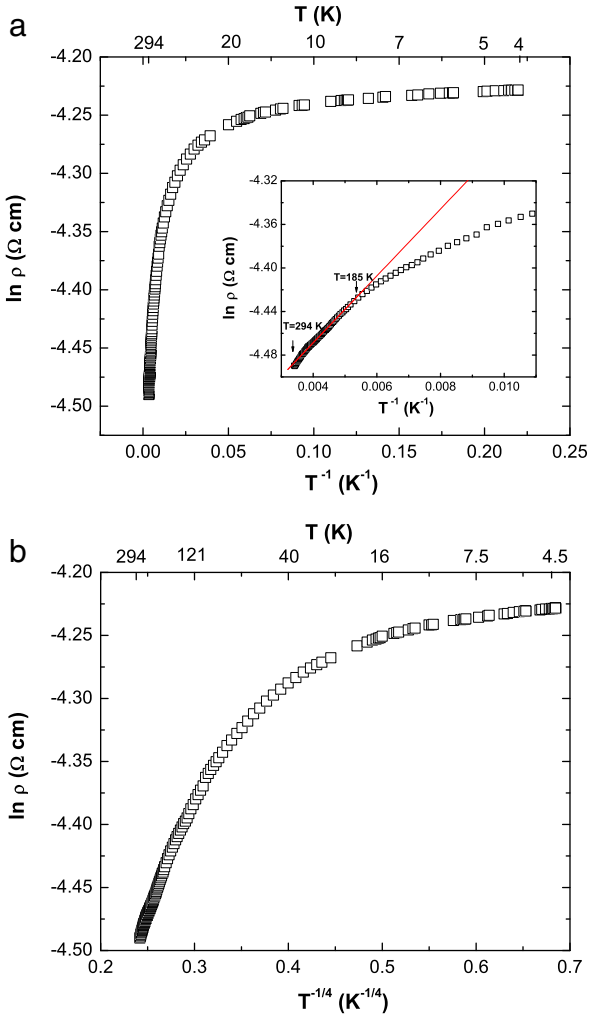

Fig. 6. a. Arrhenius plot of the normalized resistance of a ZnO thin film grown on the (100) MgO substrate at room T. The inset shows the variation in the 294 to 185 K range on an expanded scale. b. The variation of the ln ρ in function of $T^{-1/4}$.

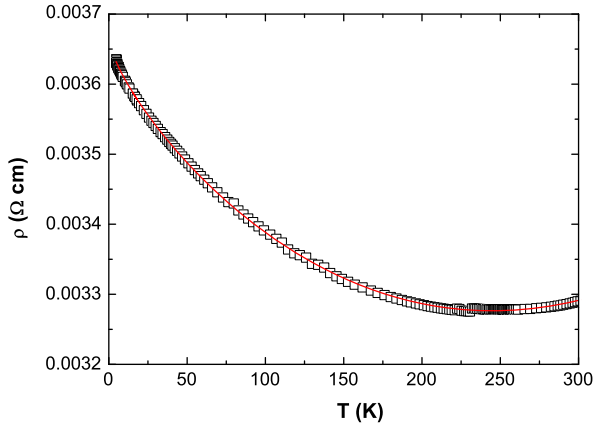

Fig. 7. Temperature dependence of the resistivity ρ(T) of ZnO grown on the (100) MgO substrate at 300 °C by PED. The solid line is the fit with the Eq. (1) of the experimental data (open rectangles).

Λ ($h / \rho n e^2 \lambda_F$) are comparable, where n is the carrier density, ρ the resistivity and e the electron charge [14,32]. In this work, with the values of resistivity (ρ) and electron density (n) measured by Hall effect measurements at room T for the ZnO film grown at 300 °C ($\rho = 0.0033\ \Omega$cm, $\mu = 12.94$ Vcm^2/s and $n = 1.45 \times 10^{20}$ cm^{-3}) and 500 °C ($\rho = 0.0023\ \Omega$cm, $\mu = 14.12$ Vcm^2/s and $n = 1.95 \times 10^{20}$ cm^{-3}) the validity of the model was checked, λ_F and Λ being comparable ($\lambda_{F\ 300} = 3.9$ nm, $\Lambda_{300} = 1.9$ nm and $\lambda_{F\ 500} = 3.5$ nm, $\Lambda_{500} = 1.7$ nm, respectively).

This model leads to a relatively high value of the transition temperature corresponding to the minimum of the resistivity ($T_m = 240$ K for the ZnO film grown at 300 °C and 186 K for the ZnO film grown at 500 °C) but similar values of the T_m were already reported for other oxide films: Ga doped ZnO ($T_m = 170$ K) [21], B doped ZnO ($T_m = 120$ K) [27], undoped ZnO ($T_m = 170$ K) [14], indium-tin oxide ($T_m = 175$ K) [33] and non-polar ZnO films [34]. In order to check the validity of the model at such higher T_m the quantum corrections were compared to the Boltzmann conductivity in the range 10–250 K ($\delta\sigma = a_1 T^{p/2} + a_2 T^{1/2} << \sigma_0$). The values of the quantum corrections obtained from the fit (Fig. 8) give a ratio $\delta\sigma/\sigma_0 < 0.1$ and are much smaller than the values corresponding to the Boltzmann conductivity [32]. The fact that the Boltzmann conductivity variation with temperature (bT^2 term) is very limited in this temperature range (due to the low b value deduced from the fit) leads to a variation of the Boltzmann conductivity lower than 1% in the 10–250 K range. So, even with limited values, the quantum corrections can overcome this low variation in Boltzmann conductivity and can lead to the high transition temperature T_m.

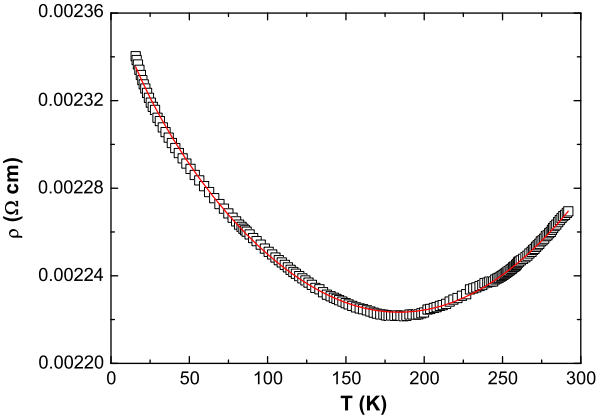

Fig. 8. Temperature dependence of the resistivity ρ(T) of ZnO grown on the (100) MgO substrate at 500 °C by PED. The solid line is the fit with Eq. (1) of the experimental data (open rectangles).

4. Discussion

The ZnO films grown by PED on MgO substrates show a preferred c-axis orientation, while the published results on ZnO films grown by other methods report a wide variety of orientations [2,6–8]. The strong (00·2) texture observed in this work has to be explained and in this aim, the effects of the surface free energy have to be considered. Indeed, if γ_f, γ_s and γ_i are the free energy for the film–ambient, substrate–ambient and film–substrate interface respectively, and γ_e the epitaxial energy gain, the increase of surface free energy due to the presence of the film is given by:

$$G = (\gamma_f - \gamma_s) + (\gamma_i - \gamma_e)$$

and the film grows in a way to minimize the free energy G [35]. First, the (00·2) ZnO texture was observed in films presenting or not epitaxial relationships with the MgO substrates. The term γ_e does not seem thus to play a major role on the ZnO film texture.

In the ZnO wurtzite structure, the (00·2) plane is a polar plane, i.e. alternate planes of Zn and O. The surface free energy of such planes will diverge as it has been shown [36]. By comparison the prismatic planes of this wurtzite structure have a lower surface free energy. In a first approach, solely based on energy considerations, the growth of ZnO films should occur with a prismatic plane ((10·0) or (11·0) for example) parallel to the substrate surface, whatever be the substrate. However, kinetics effects are present during the film formation, and the very high growth rate of ZnO along the c-axis leads to a columnar growth for ZnO which is observed on various substrates [1,37], despite the unfavourable surface free energy of the (00·2) plane. On the contrary, the (10·0) or (11·0) ZnO texture would lead to a 2D like growth, i.e. a platelet like structure, and should only be obtained in the case of a low growth rate or deposition rate. These conditions are fulfilled in the growth by molecular beam epitaxy, and the formation of m oriented ZnO films on MgO substrates has been reported in these conditions [7]. A high flux of incident species on the substrate, which is a characteristic of the pulsed deposition methods, will favour a high growth rate and therefore the formation of polar (00·2) ZnO films can be expected by PED.

Another important factor can play a role on the precise ZnO film texture, i.e. the rumpling phenomenon described above. This phenomenon will be equivalent to the creation of an electronegative surface plane (polar plane), which will result in the deposition of an electropositive Zn plane, i.e. a polar plane as the (00·2) ZnO plane. This explanation of the ZnO film orientation related to the polar nature of the substrate surface is very similar to what was recently proposed in the growth of ZnO on $SrTiO_3$ substrates [3,4]. Generally, non polar (11·0) oriented ZnO films are grown on (001) oriented $SrTiO_3$ substrates, however a c-axis columnar growth is observed on etched (001) oriented $SrTiO_3$ substrates. This change in ZnO growth direction is believed to be caused by the change of $SrTiO_3$ polarity induced by the etching [5].

The metallic conductivity observed in the ZnO films can be explained by the formation of a degenerate band appearing in heavily doped semiconductors [20,38]. Hall measurements performed on these films gave carriers densities in the 10^{20} cm^{-3} ranges, i.e. values sufficient to give rise to this effect [39]. In addition, the crossover from metallic to semiconducting behaviour has been interpreted by the quantum corrections to conductivity in disordered conductors [15]. The two pertinent points for the occurrence of MST are thus a sufficient high density of carriers and a sufficient density of structural defects in the films. In the case of ZnO films doped by various elements [20,21,25–27], the density of carriers is related to the presence of dopants. In the present case, noticeable incorporations of foreign

Table 3
Values of the fit parameters of Eq. (1) for ZnO films grown on (100) MgO substrates at 300 and 500 °C, respectively.

Substrate temperature	Fit parameters				
	$1/\rho_0$ ($\Omega^{-1}cm^{-1}$)	a_1 ($\Omega^{-1}cm^{-1}K^{-p/2}$)	p	a_2 ($\Omega^{-1}cm^{-1}K^{-1/2}$)	B ($\Omega^{-1}cm^{-1}K^{-2}$)
300 °C	272.4 ± 0.05	0.2 ± 0.001	2	1.0 ± 0.02	$3.6 \times 10^{-9} \pm 2.8 \times 10^{-11}$
500 °C	419.2 ± 0.2	0.009 ± 0.0002	3	2.1 ± 0.04	$4.0209 \times 10^{-9} \pm 4.9 \times 10^{-11}$

atoms in the ZnO films has not been evidenced, but owing to the sensitivity of RBS analysis, we cannot *a priori* exclude that a very small amount of elements is present and could thus contribute to the high density of carriers. On the other hand, even if measurable oxygen deficiencies have not been evidenced by RBS, the oxygen pressure during the growth, estimated around 10^{-3} Pa would be sufficiently low to lead to limited oxygen incorporation in the films [18], i.e. to the presence of oxygen vacancies. This oxygen deficiency can explain the rather high carrier densities determined by Hall effect measurements (about 10^{20} cm^{-3}) in these films.

One part of the disorder in the PED grown ZnO films may be related to the oxygen vacancies due to the growth process. Indeed, these oxygen vacancies could be at least partly at the origin of ZnO cell distortion in the films. Moreover, the high deposition rates observed in PED [9], which plays a role on the film growth texture (see above), can also be at the origin of the disorder created in the ZnO films. Indeed, deposition rates as high as 1 nm per pulse are currently obtained during PED growth, thanks to the high efficiency of energy transfer from incident polyenergetic (up to 15 keV) electrons to the ZnO target. For comparison purposes, ten times lower deposition rates are obtained during another pulsed deposition process, pulsed laser deposition. With such high deposition rates, the crystalline quality of the grown films cannot be guaranteed, as it can be checked through the difference in ZnO axis parameter with bulk value, width of the diffraction peak and FWHM values of the (00·2) rocking curve, observed in this work.

5. Conclusions

In summary, the pertinent factors allowing the formation by PED of (00·2) rhombohedral ZnO textured films on (100) MgO substrates are (i) the high deposition rate (high flux of incident species) favouring the high (00·2) ZnO growth rate, and (ii) the rumpling phenomenon of the MgO substrate favouring the growth of the polar (00·2) ZnO plane at the surface of the substrate. The high density of crystalline defects in the ZnO films grown on (100) oriented MgO substrates over the 300–500 °C temperature range associated with the high deposition rate of the PED method is very favourable for the occurrence of the metal–semiconductor transition observed in the variable temperature resistivity curves.

Acknowledgements

The authors gratefully acknowledge financial support from the Romanian Ministry for Education, Research, Youth and Sport (Project No. 12-112/2008) and from the agreement on cooperation between INSP, Université Pierre et Marie Curie-Paris 6 and NILPRP.

References

[1] S.J. Pearton, D.P. Norton, K. Ip, Y.W. Heo, T. Steiner, Prog. Mater. Sci. 50 (2005) 293.
[2] L.C. Nistor, C. Ghica, D. Matei, G. Dinescu, M. Dinescu, G.V. Tandeloo, J. Cryst. Growth 277 (2005) 26.
[3] C.H. Jia, Y.H. Chen, G.H. Liu, X.L. Liu, S.Y. Yang, Z.G. Wang, J. Phys. D Appl. Phys. 42 (2009) 015415.
[4] M. Karger, M. Schilling, Phys. Rev. B 71 (2005) 075304.
[5] X.H. Wei, Y.R. Li, J. Zhu, W. Huang, Y. Zhang, W.B. Luo, H. Ji, Appl. Phys. Lett. 90 (2007) 151918.
[6] F.K. Shan, G.X. Liu, W.J. Lee, B.C. Shin, Integr. Ferroelectr. 78 (2006) 181.
[7] E. Cagin, J. Yang, W. Wang, J.D. Phillips, S.K. Hong, J.W. Lee, J.Y. Lee, Appl. Phys. Lett. 92 (2008) 233505.
[8] M.W. Cho, A. Setiawan, H.J. Ko, S.H. Kong, T. Yao, Semicond. Sci. Technol. 20 (2005) S13.
[9] M. Nistor, N.B. Mandache, J. Perrière, J. Phys. D Appl. Phys. 41 (2008) 165205.
[10] R.J. Choudhary, S.B. Ogale, S.R. Shinde, V.N. Kulkarni, T. Venkatesan, K.S. Harshavardhan, M. Strikovski, B. Hannoyer, Appl. Phys. Lett. 84 (2004) 1483.
[11] M. Nistor, P. Charles, M. Ganciu, M. Lamoureux, N.B. Mandache, A.M. Pointu, Plasma Sources Sci. Technol. 11 (2002) 183.
[12] M. Nistor, F. Gherendi, M. Magureanu, N.B. Mandache, A. Ioachim, M.G. Banciu, L. Nedelcu, M. Popescu, F. Sava, H.V. Alexandru, Appl. Surf. Sci. 247 (2005) 169.
[13] M. Nistor, J. Perrière, C. Hebert, W. Seiler, J. Phys. Condens. Matter 22 (2010) 045006.
[14] M. Nistor, F. Gherendi, N.B. Mandache, C. Hebert, J. Perrière, W. Seiler, J. Appl. Phys. 106 (2009) 103710.
[15] P.A. Lee, T.V. Ramakrishnan, Rev. Mod. Phys. 57 (1985) 287.
[16] M. Nistor, N.B. Mandache, J. Optoelectron. Adv. Mater. 7 (2005) 1619.
[17] M. Nistor, F. Gherendi, M. Magureanu, N.B. Mandache, J. Optoelectron. Adv. Mater. 7 (2005) 979.
[18] R. Perez-Casero, A. Gutierrez-Llorente, O. Pons-Y-Moll, W. Seiler, R.M. Defourneau, D. Defourneau, E. Millon, J. Perrière, J. Appl. Phys. 97 (2005) 054905.
[19] R. Perez-Casero, J. Perrière, A. Gutierrez-Llorente, D. Defourneau, E. Millon, W. Seiler, L. Soriano, Phys. Rev. B 75 (2007) 165317.
[20] V. Bhosle, A. Tiwari, J. Narayan, Appl. Phys. Lett. 88 (2006) 032106.
[21] V. Bhosle, A. Tiwari, J. Narayan, J. Appl. Phys. 100 (2006) 033713.
[22] V. Craciun, R.K. Singh, J. Perrière, J. Spear, D. Craciun, J. Electrochem. Soc. 147 (2000) 1077.
[23] D.R. Alfonso, J.A. Snyder, J.E. Jaffe, A.C. Hess, M. Gutowski, Phys. Rev. B 62 (2000) 8318.
[24] J. Narayan, K. Dovidenko, A.K. Sharma, S. Oktyabarsky, J. Appl. Phys. 84 (1998) 2597.
[25] O. Bamiduro, H. Mustafa, R. Mundle, R.B. Konda, A.K. Pradhan, Appl. Phys. Lett. 90 (2007) 252108.
[26] A.K. Pradhan, L. Douglas, H. Mustata, R. Mundle, D. Hunter, C.E. Bonner, Appl. Phys. Lett. 90 (2007) 072108.
[27] X.D. Liu, E.Y. Jiang, Z.Q. Li, J. Appl. Phys. 102 (2007) 073708.
[28] C. Fournier, O. Bamidoro, H. Mustafa, R. Mundle, R.B. Konda, F. Williams, A.K. Pradhan, Semicond. Sci. Technol. 23 (2008) 085019.
[29] Y. Li, C. Li, D. He, J. Li, J. Phys. D Appl. Phys. 42 (2009) 105303.
[30] N. Kavasoglu, A.S. Kavasoglu, Phys. B 403 (2008) 2807.
[31] G. Herranz, F. Sánchez, B. Martínez, J. Fontcuberta, M.V. García-Cuenca, C. Ferrater, M. Varela, P. Levy, Eur. Phys. J. B 40 (2004) 439.
[32] W. Noun, B. Berini, Y. Dumont, P.R. Dahoo, N. Keller, J. Appl. Phys. 102 (2007) 063709.
[33] T. Ohyama, M. Okamoto, E. Otsuka, J. Phys. Soc. Jpn 54 (1985) 1041.
[34] P. Pant, J.D. Budai, R. Aggarwal, R.J. Narayan, J. Narayan, Acta Mater. 57 (2009) 4426.
[35] O. Pons, Y. Moll, J. Perrière, E. Millon, R.M. Defourneau, D. Defourneau, B. Vincent, A. Essahlaoui, A. Boudrioua, W. Seiler, J. Appl. Phys. 92 (2002) 4885.
[36] P.W. Tasker, J. Phys. C Solid State Phys. 12 (1979) 4977.
[37] V. Craciun, J. Perrière, N. Bassim, R.K. Singh, D. Craciun, J. Spear, Appl. Phys. A 69 (1999) 531.
[38] N.F. Mott, Metal Insulator Transitions, Taylor and Francis, London, 1974.
[39] A.P. Roth, J.B. Webb, D.F. Williams, Solid State Comm. 39 (1981) 1269.